IL NUOVO CIMENTO Vol. 28 C, N. 4-5 Luglio-Ottobre 2005
DOI 10.1393/ncc/i2005-10123-4

Star formation efficiency and host galaxies of Gamma-Ray Bursts(*)

S. Courty, G. Björnsson and E. H. Gudmundsson
Science Institute, University of Iceland - Dunhagi 3, IS-107, Reykjavik, Iceland

(ricevuto il 23 Maggio 2005; pubblicato online il 13 Ottobre 2005)

Summary. — Gamma-ray bursts are likely to be associated with regions of active star formation and may therefore be useful as cosmological tracers of galaxy formation. Using hydrodynamical/N-body simulations the cosmological properties of host galaxies are investigated. Assuming the hosts to be efficient star-forming objects, *i.e.* with high specific star formation rates, the majority of the candidate hosts are found to be low mass, young galaxies with a moderate star formation rate. This picture, consistent with most observations of GRB host galaxies, corroborates the idea that gamma-ray bursts do not follow the cosmic star formation rate. More importantly the hosts should contribute to unveil the faint end of the galaxy luminosity function.

PACS 98.62.Ai – Origin, formation, evolution, age, and star formation.
PACS 98.70.Rz – γ-ray sources; γ-ray bursts.
PACS 98.62.Ve – Statistical and correlative studies of properties (luminosity and mass functions; mass-to-light ratio; Tully-Fisher relation, etc.) .
PACS 01.30.Cc – Conference proceedings.

1. – Numerical simulations

In 1997 the first optical transient of a Gamma-Ray Burst (GRB) was detected, allowing a redshift determination and therefore making Gamma-Ray Bursts (GRBs) possible cosmological tracers of galaxy formation. From then around 40 redshifts have been measured for GRB afterglows and their host galaxies. Most of the hosts seem to be sub-luminous, blue galaxies with moderate optical star formation rates (*e.g.* [1-3], and references therein). We address the issue of the GRB host galaxy properties using cosmological simulations of galaxy formation.

These N-body/Eulerian hydrodynamical simulations follow the dynamical evolution of the dark matter and the baryonic matter and include gravitation, shock heating and radiative cooling without assuming the ionization-recombination equilibrium (details in [4]). Photoionization processes are not included. Galaxy formation is treated with a phenomenological description based on the selection of gas regions satisfying the following

(*) Paper presented at the "4th Workshop on Gamma-Ray Burst in the Afterglow Era", Rome, October 18-22, 2004.

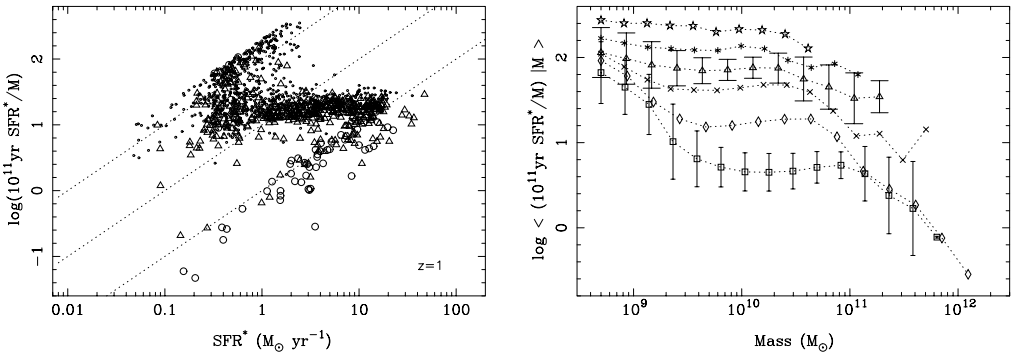

Fig. 1. – Left panel: Star formation efficiency (ϵ parameter) *vs.* activity (SFR^*) for 1000 star-forming galaxies randomly selected in the catalog at $z = 1$. Circles indicate early-formed objects and dots late-formed objects, triangles indicate intermediate epoch of formation. Diagonal lines are equal galaxy mass lines, 10^9, 10^{10}, 10^{11} $M_\odot$ (from left to right). Right panel: Conditional mean of having a specific star formation rate at a given mass, $\langle \epsilon | M \rangle$, as a function of mass at different redshifts: $z = 0$ (squares), $z = 1$ (diamonds), $z = 2$ (crosses), $z = 3$ (triangles), $z = 4$ (stars), $z = 5$ (open stars); for clarity, error bars representing dispersion around the mean are only plotted at $z = 0$ and $z = 3$.

criteria: cooling time less than the dynamical time ($t_{\rm cool} < t_{\rm dyn}$), cell size larger than Jean's scale ($\lambda < \lambda_{\rm J}$), convergent flow ($\nabla \cdot \vec{v} < 0$), baryonic density contrast higher than a given threshold ($\delta_{\rm B} \equiv (\delta\rho/\bar{\rho})_{\rm B} > 5.5$). A gas fraction of the selected cells is turned into a stellar particle with mass $m_* = m_{\rm B}(t)\Delta t/\max(t_{\rm dyn}, 10^8$ y) and the epoch of formation is recorded; here $m_{\rm B}(t)$ denotes the amount of gas present in a cell at time t. The subsequent evolution of the stellar particles is followed in a non-collisional way and at any given redshift, galaxies are defined by grouping the stellar particles with a friend-of-friend algorithm. Galaxies are characterized at any redshift by the following properties: Mass: sum of the masses of all the stellar particles the galaxy is composed of; Epoch of formation: the mass-weighted average of the epochs of formation of all the stellar particles contained in a galaxy; Instantaneous star formation rate (SFR^*): the amount of stellar material formed over 10^8 y before a given redshift. We also estimate the specific star formation rate, which is the ratio between the SFR^* and the mass of the galaxy, using the parameter $\epsilon \equiv \log[(SFR^*/M_\odot {\rm y}^{-1})(M/10^{11} M_\odot)^{-1}]$. We include in the simulated catalogs all galaxies with $M > 5 \times 10^8$ $M_\odot$. The simulation parameters are the following: the number of dark matter particles is 256^3, as are the number of grid cells; the comoving size of the computational volume is $L = 32$ h^{-1} Mpc; the dark matter particle mass is $M_{DM} = 2.01 \times 10^8$ $M_\odot$; the initial gas mass per grid cell is $M_{BM} = 3.09 \times 10^7$ $M_\odot$. The results are given for a ΛCDM cosmological scenario: $\Omega_m = 0.3$, $\Omega_\Lambda = 0.7$, $\Omega_b h^2 = 0.02$, $h = (H_0/100) = 0.7$, $\sigma_8 = 0.91$.

The left panel of fig. 1 displays galaxies at low redshift in a specific SFR-SFR^* diagram using different symbols for the epoch of formation. Distinct sub-populations of galaxies are clearly seen: For instance, high-mass, old galaxies with low SFR^*, or high-mass galaxies with high SFR^* and intermediate epochs of formation. The interesting point is that the high-mass, old galaxies can have as low SFR^* as the low-mass, young galaxies, but this latter population has higher specific SFRs than the former one. This diagram nicely underlines two different notions of the galaxy formation process: The SFR^* measures the amount of gas turned into stellar material whereas the specific SFR is a measurement of how efficient this conversion is. We emphasize that this diagram

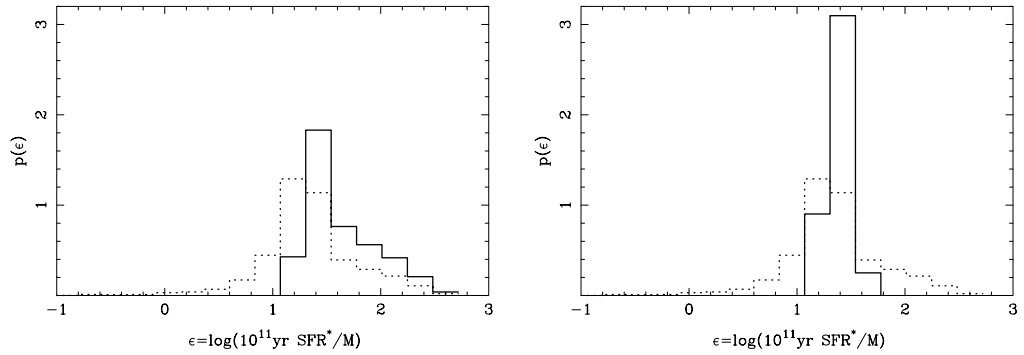

Fig. 2. – Left panel: Probability density functions of the specific star formation rate for the host galaxy population (solid) and the overall galaxy population (dotted) at $z = 1$. Right panel: same but the solid line is now the host population with low-mass galaxies, $M < 10^{10}\ M_{\odot}$, excluded.

only displays the star-forming galaxy population: A number of galaxies, especially at low redshift, have a $SFR^* = 0$. These galaxies, either low-mass or high-mass galaxies but with old epochs of formation, are likely to have ceased or slowed down their star formation activity. Those high-mass, old galaxies with a null SFR^* are located in the center of the biggest dark matter halos found in the simulations. The right panel of fig. 1 shows the cosmological evolution of the specific star formation rate. It tends to decrease at a given mass as the redshift decreases and shows a larger dispersion at low redshift due to the evolution effects, suggesting that the SFR is no more a linear function of the galaxy mass.

2. – Candidate GRB host galaxies

We select GRB host candidates among the simulated objects as galaxies with specific star formation rates higher than a given threshold, whose value is dependent on redshift. Selecting host candidates as the most efficient galaxies, for instance with $\epsilon > 1.3$ at $z = 1$ (see left panel of Fig. 1), leads to the conclusion that hosts are low-mass or intermediate-mass galaxies, rather young, and with SFR^* ranging between 0.01 and 50 $M_{\odot}\ \mathrm{y}^{-1}$. Increasing the threshold value would select only low-mass galaxies with moderate SFR^*, up to $\sim 3\ M_{\odot}\ \mathrm{y}^{-1}$.

The left panel of fig. 2 displays the distribution of the specific star formation rate computed for the host population, clearly different from the distribution for the overall population. The latter distribution is compared in the right panel with the distribution computed for the host population but excluding now the low-mass host candidates ($M < 10^{10}\ M_{\odot}$). The distribution for the hosts is now quite different from the host distribution in the left panel and peaks around intermediate specific SFRs. This distribution resembles the results of a number of current observations. For instance it is shown in [5] that "67% of the HDF galaxies classified as starburst galaxies have specific SFRs of more than $5\ M_{\odot}\ \mathrm{y}^{-1}\ (L/L^*)^{-1}$", which is the lowest value of their host galaxy sample. Moreover their sample shows a narrow range of SFR/L values, which might suggest a lack of faint host galaxies. Therefore fig. 2 emphasizes that if GRBs occur in very efficient galaxies we should expect to detect lower mass/fainter galaxies. We have also estimated the distribution of the specific star formation rate for the youngest simulated galaxies and find that it is much closer to the host distribution in the left panel.

Assuming on the other hand that GRB host candidates are galaxies with high star

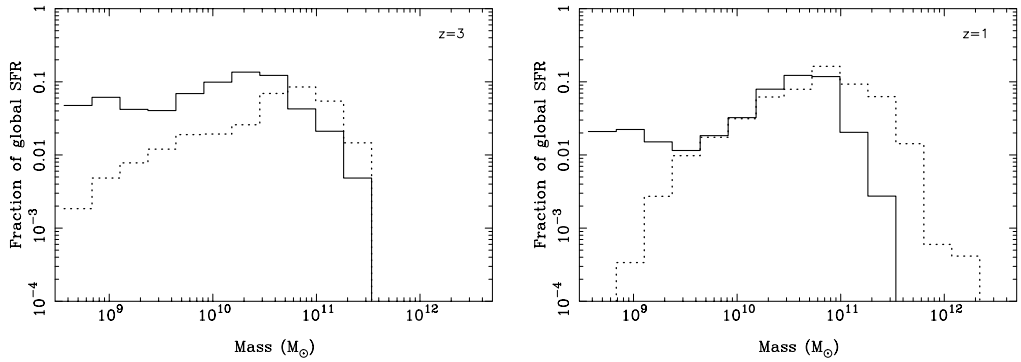

Fig. 3. – Contribution to the global SFR per bin of mass at $z = 3$ (left panel) and $z = 1$ (right panel) for the galaxy population with $\epsilon < \epsilon_{th}(z)$ (dotted line) and $\epsilon > \epsilon_{th}(z)$ (solid line).

formation rates (for instance $SFR^* > 5$ in the left panel of fig. 1) would lead to the conclusion that hosts are intermediate or high-mass galaxies, with epochs of formation and specific star formation rates spanning a broad range of values. Our first assumption is by far the most consistent with the current observations. The cosmological evolution of the specific SFR has been discussed in the previous section and candidate hosts are selected at $z = 3$ as galaxies with $\epsilon > 1.8$. It is interesting to note that high-mass host galaxies at $z = 3$ may have similar specific SFRs as low-mass hosts at $z = 1$. This result is consistent with the observations in [6]: The specific SFR of the single host at $z = 3$ in their sample is similar to the specific SFRs of their six low-mass hosts at $z = 1$. Here again the simulations suggest that low-mass galaxies should be detected with high specific SFRs at high redshift. Many details of the results discussed above can be found in [7].

The *SWIFT* satellite, dedicated to the observation of GRBs will increase the sample of host galaxies and allow a more accurate estimate of the selection biases. How host galaxies are distributed in the specific SFR-SFR^* diagram will certainly give some clue about this particular population: Measuring high specific SFRs and low masses might rule out the idea that the GRB formation rate follows the cosmic SFR *at low redshift*. Figure 3 shows that low-mass galaxies do not contribute to the total SFR at $z = 1$ (in fact 50% of the total SFR is in galaxies with $\epsilon > 1.3$ at $z = 1$), but that this contribution increases at high redshift. It is also interesting to note that high-mass galaxies are neither the major contributor to the total SFR at $z = 1$. But more importantly GRBs are appearing as a unique tracer of a part of the faint galaxy population, whose study is crucial for our understanding of the galaxy formation process.

REFERENCES

[1] Berger E., Cowie L. L., Kulkarni S. R., Frail D. A., Aussel H. *et al.*, *ApJ*, **588** (2003) 99.
[2] Jaunsen A. O., Andersen M. I., Hjorth J., Fynbo J. P. U., Holland S. T. *et al.*, N. R., *A&A*, **402** (2003) 125.
[3] Le Floc'h E., Duc P.-A., Mirabel I. F., Sanders D. B., Bosch G. *et al.*, *A&A*, **400** (2003) 499.
[4] Teyssier R., Chièze J.-P. and Alimi J.-M.,*ApJ*, **509** (1998) 62.
[5] Christensen L., Hjorth J. and Gorosabel J., *A&A*, **425** (2004) 913.
[6] Chary R., Becklin E. E. and Armus L., *ApJ*, **566** (2002) 229.
[7] Courty S., Björnsson G. and Gudmundsson E. H., *MNRAS*, **354** (2004) 581.